Porosity in Subsoil Rock: Rates of Formation, Kinds of Pores, and Biotic Access

Robert C. Graham[1]*, Ann M. Rossi[1], Michael F. Allen[1], Ranjith P. Udawatta[2], Clark J. Gantzer[3], Stephen H. Anderson[3], Richard A. Ketcham[4]

Project Objectives

(1) Measure the rate of porosity formation in granitic rock.
(2) Characterize the nature of the porosity (size, shape, distribution of pores).

Approaches and Procedures

Rock fragments (clasts) were sampled from seven moraines in the Bishop Creek Moraine sequence (Table 1). Moraines sampled range in age from 15 – 170 ka. Surface ages of the moraines correspond to the time of weathering for clasts deposited within the moraine. Total porosity of each clast was estimated from bulk density and particle density measurements. Thin sections made from clasts were studied to characterize pore morphology and mineral weathering characteristics.

Selected samples of rock and soil material (Table 1) were scanned at the High Resolution X-Ray CT facility at the University of Texas, Austin. Soil materials were included for comparison. The X-ray scanner settings yielded a spot size of about 50 μm. Slice thickness and slice spacing were both 42.4 μm producing a volume element (voxel) of $6.4*10^4$ μm^3. Contiguous scans were stacked to render 3-D volumes. From each sample, a 480*480*580 data block was extracted for image analysis. The 3DMA software was used for three-dimensional quantification of pore characteristics (Lindquist, 1999; Lindquist and Venkatarangan, 1999). A number of algorithms are imbedded in the image analysis software to accomplish the six main steps: segmentation of image, extraction and modification of the medial axis of pore paths, throat construction using the medial axis, pore surface construction, assembly of pore throat network, and geometrical characterization of pore throat network. Analysis followed information outlined in Lindquist et al. (2005) and generated information for porosity; as well as corresponding probabilities for coordination numbers, path lengths, pore volume, effective radii, and path tortuosity. Analysis of variance and t-tests were conducted to compare differences in porosity, pore connectivity, path length, pore volume, pore radii and tortuosity among treatments to examine the effect of weathering. Differences were declared to be significant at $\alpha = 0.05$ level (SAS, 1999). In addition, statistical significance or numerical differences were specified within each section.

[1]University of California, Riverside

[2]Center for Agroforestry and Department of Soil, Environmental and Atmospheric Sciences, School of Natural Resources, University of Missouri, Columbia, MO 65211, USA.

[3]Department of Soil, Environmental and Atmospheric Sciences, School of Natural Resources, University of Missouri, Columbia, MO 65211, USA.

[4]Jackson School of Geosciences, University of Texas, Austin, TX 78712-1100, USA.

*Principal Investigator

For more information contact Dr. Robert Graham (robert.graham@ucr.edu)

Table 1. *Site characteristics of sampled moraines at Bishop Creek, California.*

Moraine†	Glacial Advance†	Surface Age§	Elevation	Vegetation¶	Soil	Samples for CT
		ka	m			
Ti4	Tioga 4	15.2	2482	*P. tridentata, A. tridentata, E. nevadensis, C. ledifolius, P. monophylla, P. andersonii*	loamy-skeletal, mixed, superactive, frigid Typic Haploxeroll	SHb14
Ti1	Tioga 1	24.3	2006	*P. tridentata, A. tridentata, E. nevadensis, C. ledifolius, P. monophylla*	loamy-skeletal, mixed, superactive, mesic Typic Haploxerept	SCb05
Ta5	Tahoe 5	58.0	1818	*E. nevadensis, A. tridentata, E. nauseosus, C. ramosissima*	loamy-skeletal, mixed, superactive, mesic Xeric Haplocambid	BUb02
Ta4	Tahoe 4	78.5	1708	*S. speciosa, E. pringlei, E. nevadensis, C. ramosissim, M. laevis, G. spinosa, E. cooperia, E. teretifolia*	sandy-skeletal, mixed, mesic Xeric Haplocambid	BISAb03, BISAb06
Ta2-1	Tahoe 2	119.5	1800	*E. nauseosus, E. nevadensis, B. tectorum, G. spinosa*	sandy, mixed, mesic Xeric Haplocambid	YTHb43b, YTHb44a, YTH 16-28 (soil)
Ta2-2	Tahoe 2	110.3	1629	*E. nevadensis, A. tridentata, E. nauseosus, C. ramosissima*	sandy-skeletal, mixed, mesic Xeric Haplargid	
Ta1	Tahoe 1	100.2	1833	*E. nauseosus, E. nevadensis, C. ramosissima*	loamy-skeletal, mixed, active, mesic Xeric Haplargid	OTHa13, OTHb11, OTH 10-40 cm (soil)

†Moraine names and glaciations were assigned by Phillips et al. (2009)

§Surface age is the average cosmogenic ^{36}Cl surface exposure age for all boulders sampled on the moraine (Phillips et al., 2009)

¶Common names: *Artemisia tridentata* = big sagebrush, *Bromus tectorum* = cheatgrass, *Cercocarpus ledifolius* = curl-leaf mountain mohagany, *Coleogyne ramosissima* = blackbush, *Ericameria cooperia* = Cooper's goldenbush, *Ericameria nauseosus* = rubber rabbitbrush, *Ericameria nevadensis* = Morman tea, *Eriophyllum pringlei* = Pringle's woolly daisy, *Ericameria teretifolia* = green rabbitbush, *Grayia spinosa* = spiny hopsage, *Mirabilis laevis* = wishbone bush, *Prunus andersonii* = desert peach, *Pinus monophylla* = piñon pine, *Purshia tridentata* = antelope bitterbrush, *Stipa speciosa* = desert needle grass.

Results

Total Porosity

Total porosity was measured on all clasts; however weathering characteristics were highly dependent on mineralogy. We chose to focus on weathering processes and porosity formation in the medium-grained (2-5 mm grain size) granitic clasts, as this lithology was the most common and showed the most consistent weathering across the chronosequence. Average porosity measured in clasts from each moraine and rate of porosity formation is shown in Figure 1. Total porosity ranged from 1.2% to 24.7% (data not shown). Average porosity of clasts from soils on the oldest moraine surfaces (Ta1, Ta2) ranged from 12.6 to 14.1%. The surface ages of the moraines are likely much younger than the moraine deposition ages due to erosion (Phillips et al., 2009). Surface ages are considered a better estimate of the duration of clast weathering than the moraine age, since erosion rates are variable across the moraine sequence. Rate of porosity formation has been approximately 0.10% per ka. Clasts with 8% or more porosity were easily crumbled by hand into sand and gravel fragments. Even though these clasts were permeated by a network of mesofractures (10-300 µm wide), they maintain the original rock texture and individual mineral grains are not extensively chemically altered. Material of this kind has been termed *saprock* (Anand and Paine, 2002). Field and laboratory observations revealed mycorrhizal hyphae within mesofractures of most, if not all, weathered clasts.

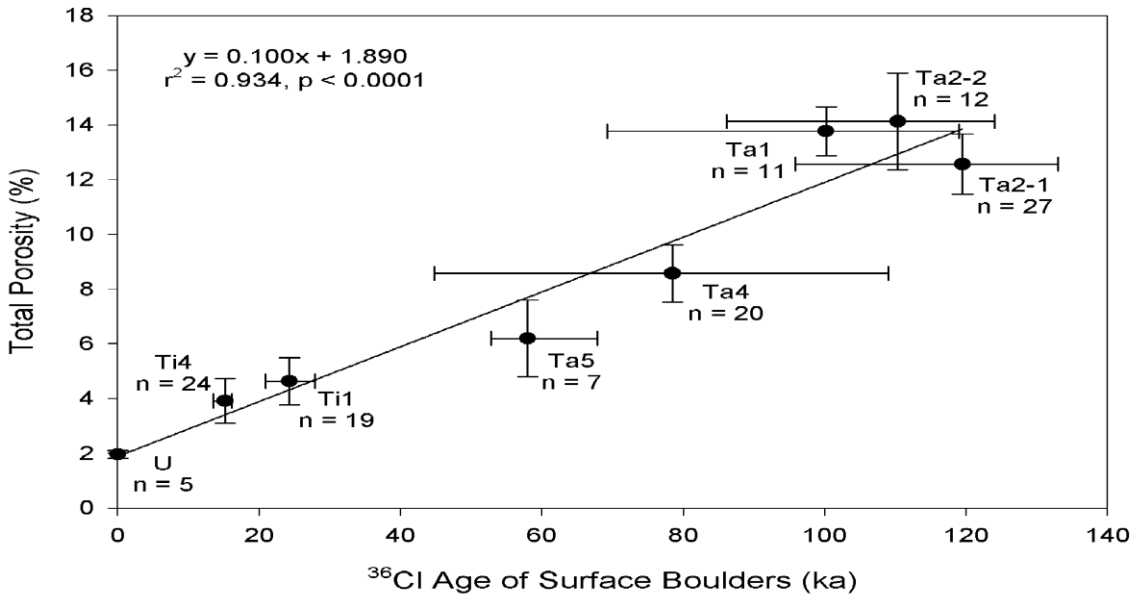

Figure 1. Total porosity of granitic clasts as a function of surface exposure age. Surface exposure age is the average cosmogenic ^{36}Cl surface exposure age measured on boulders on the moraine crest. Vertical error bars represent the standard error of the porosity. Horizontal error bars show the range of surface exposure ages measured by Phillips et al. (2009).

Thin Section Micromorphology

Thin section observations showed the number, size, and connectivity of pores increased with moraine age. Porosity consists of inter- and intramineral planar voids (Bullock et al., 1985). Initially pores are narrow, have sharp edges and are angular. As clasts weather, pores are larger and appear more rounded (Figure 2). Porosity in biotite grains is oriented parallel to cleavage planes (Figure 3). Pores become larger as biotite layers expand with increased weathering. Fracturing is common throughout quartz grains (Figure 4a,b). Pores are randomly oriented through the grain. Quartz grains do not show any evidence of chemical weathering. Fractures in feldspar grains are mostly random, however some pores trace cleavage planes for short distances (Figure 4c). Feldspar grains show little evidence of chemical weathering and transformation. The number and thickness of clay films increase in clasts from older moraines (Figure 5).

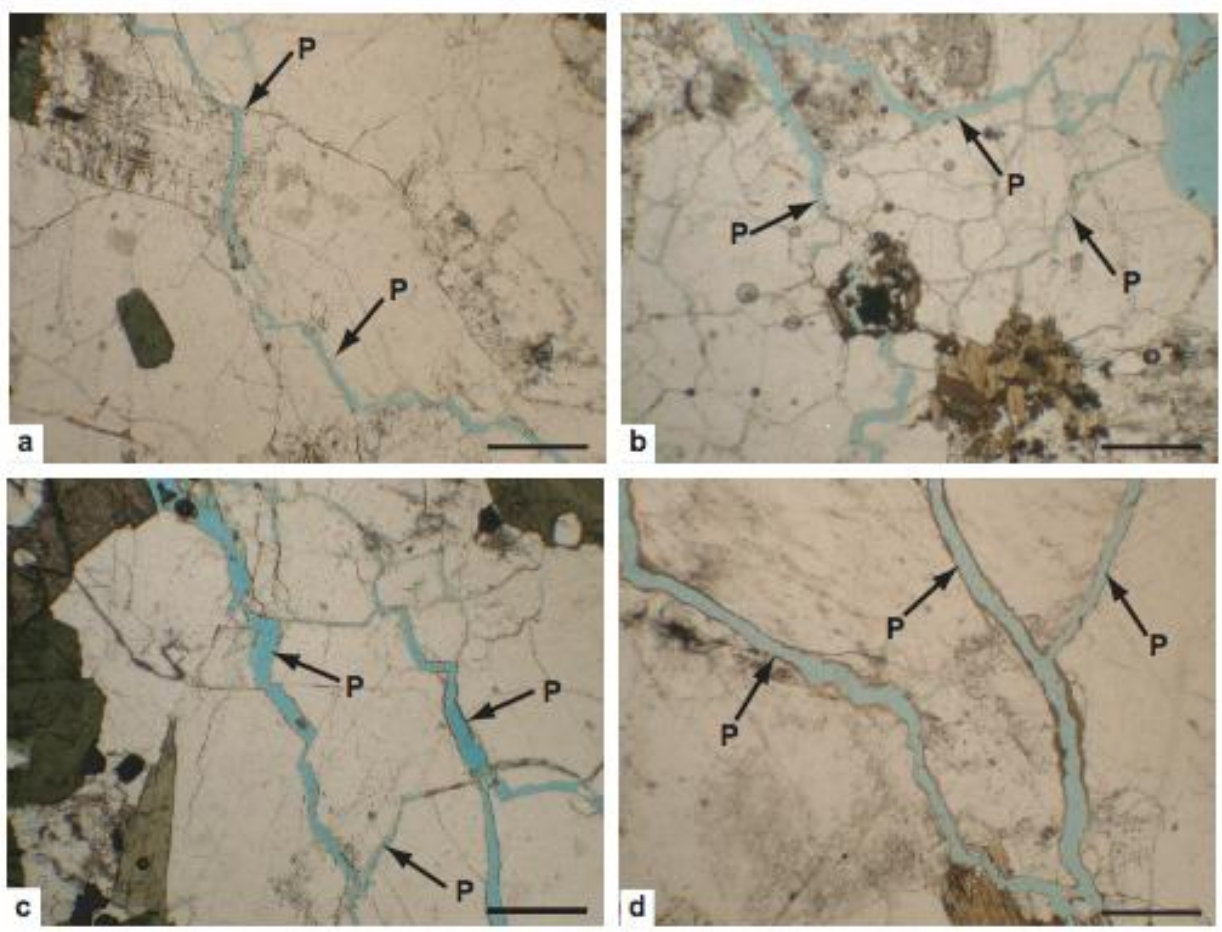

Figure 2. Thin section micrographs displaying changes in pore morphology. Scale bars equal 500 µm. Porosity (P) has been dyed blue and is indicated by arrows. (a) Ti4, (b) Ta4, (c) Ta2-1, (d) Ta1.

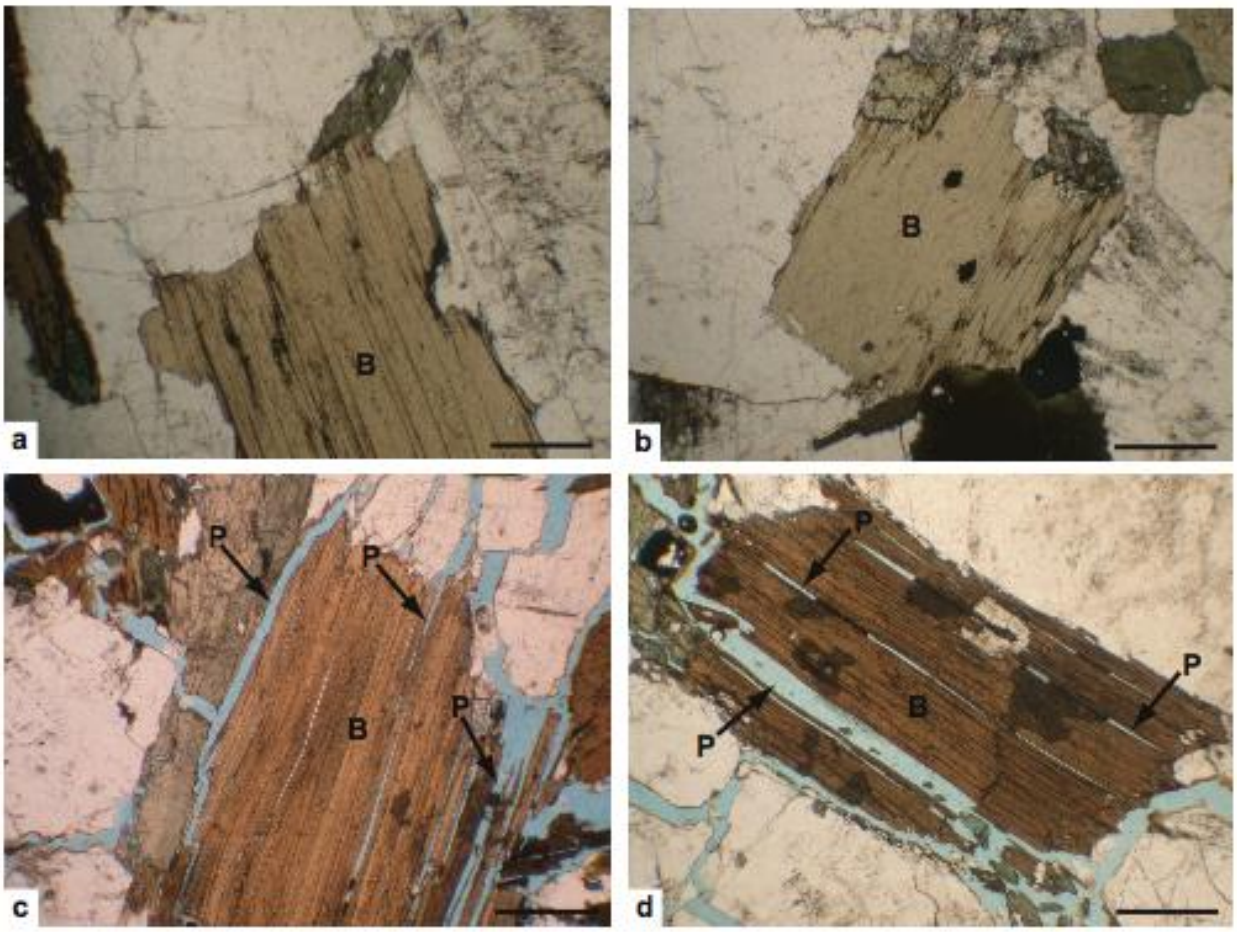

Figure 3. Thin section micrographs displaying biotite (B) expansion. Porosity (P) is dyed blue and indicated by arrows. Scale bars equal 500 µm. (a) Ti4, (b) Ta5, (c) Ta2-1, (d) Ta1.

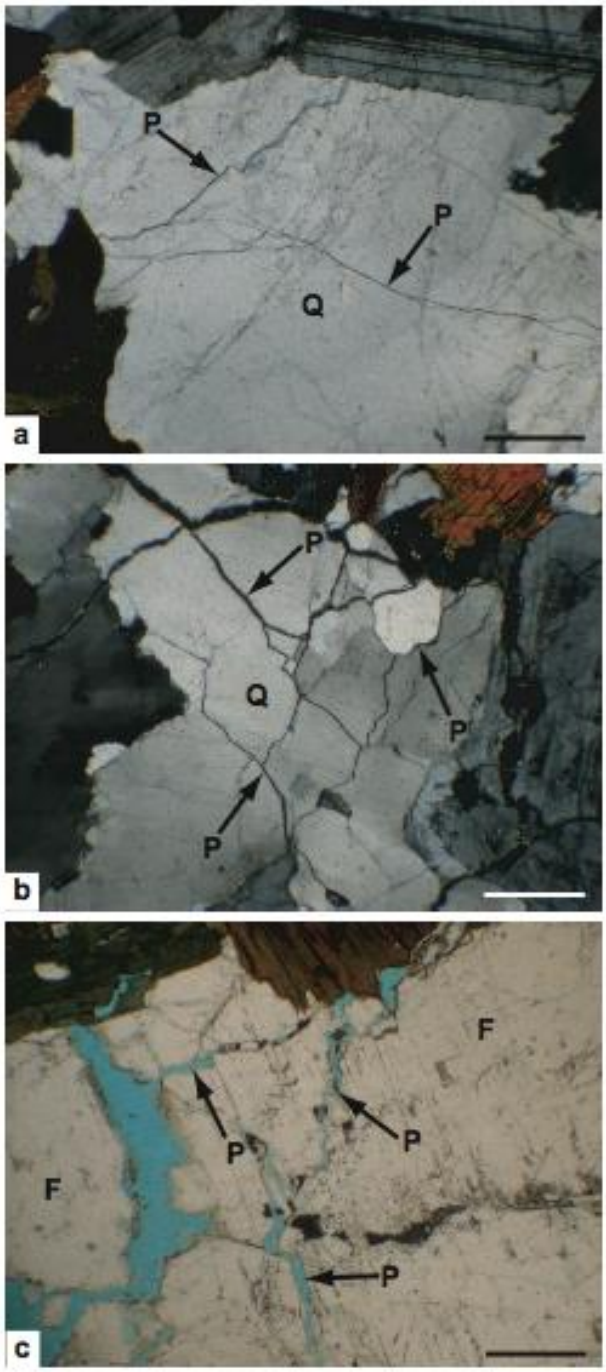

Figure 4. Thin section micrographs displaying porosity patterns. Scale bars equal 500 µm. (a) Ti1, quartz (Q) grain under cross polarized light, porosity (P) indicated by arrows, (b) Ta1, quartz (Q) grain under cross polarized light, porosity (P) indicated by arrows, (c) Ta2-1, feldspar (F) grain under plane polarized light, porosity (P) is dyed blue and indicated by arrows.

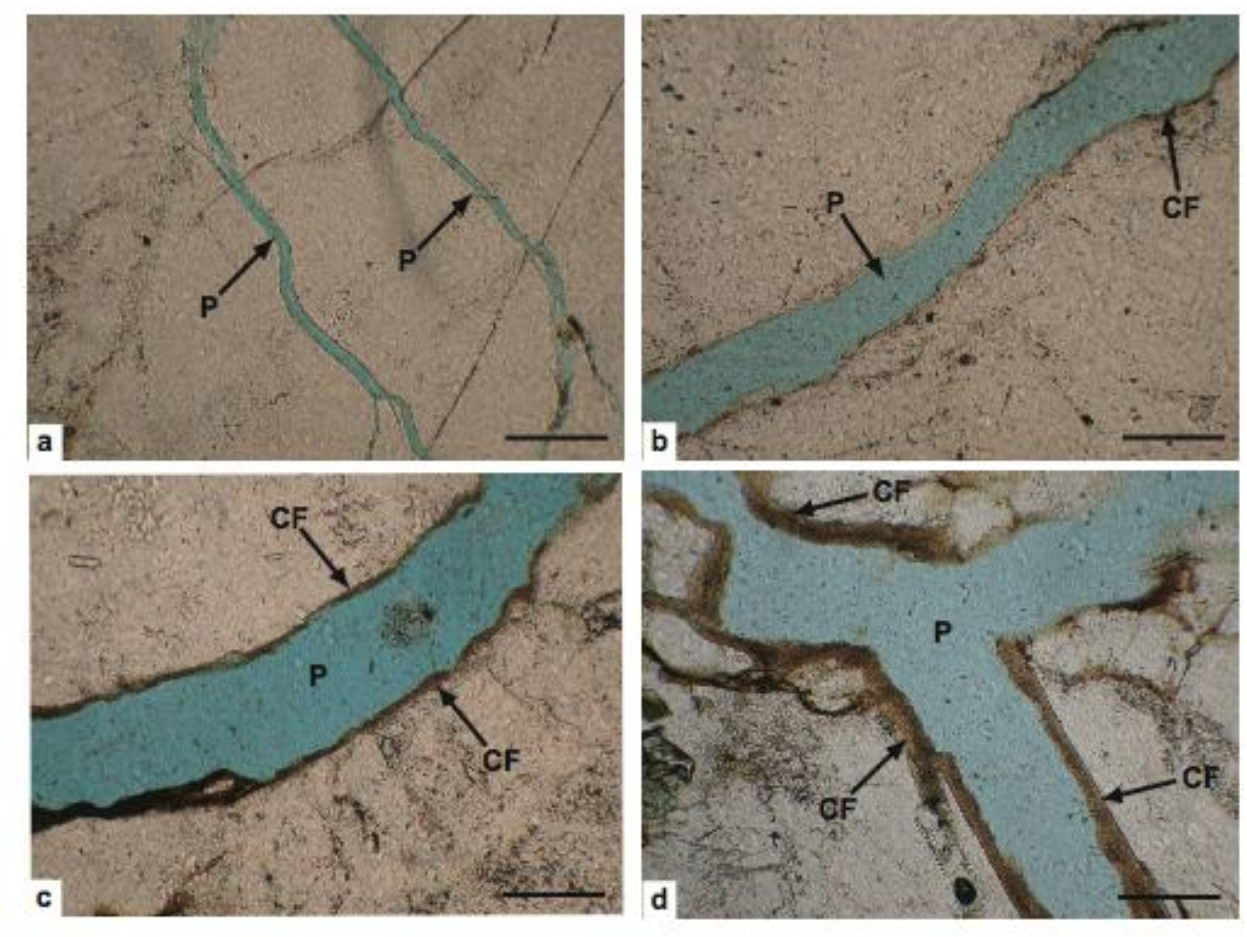

Figure 5. Thin section micrographs showing clay films (CF) along pores (P) indicated by blue dye. Scale bars equal 100 µm. (a) Ti1, (b) Ta4, (c) Ta2-1, (d) Ta1.

CT Analysis of Porosity

CT scans illustrating fracture and porosity development as a function of rock weathering time are shown in Figure 6. Clasts with bulk density-measured porosities < 5.5% were incorrectly resolved by the 3DMA procedure, thus clasts from the youngest moraines, 15 and 24 ka, had anomalously high (47 and 75%) porosities (Fig. 7). Excluding the outlying samples from the 15 and 24 ka moraines, the average 3DMA-measured porosity was 4% higher than the porosity measured by the bulk density method, as a result of partial volume effect and beam hardening. A t-test indicated no significant difference between values from the two methods and the trend across the chronosequence was similar for both procedures; i.e., porosity increases with moraine surface age. A regression relationship between the two methods was significant and explained 69% of the variation in the 3DMA values by the porosity from the bulk density method (Fig. 8). The analysis excluded the youngest two clast samples and the two soil samples.

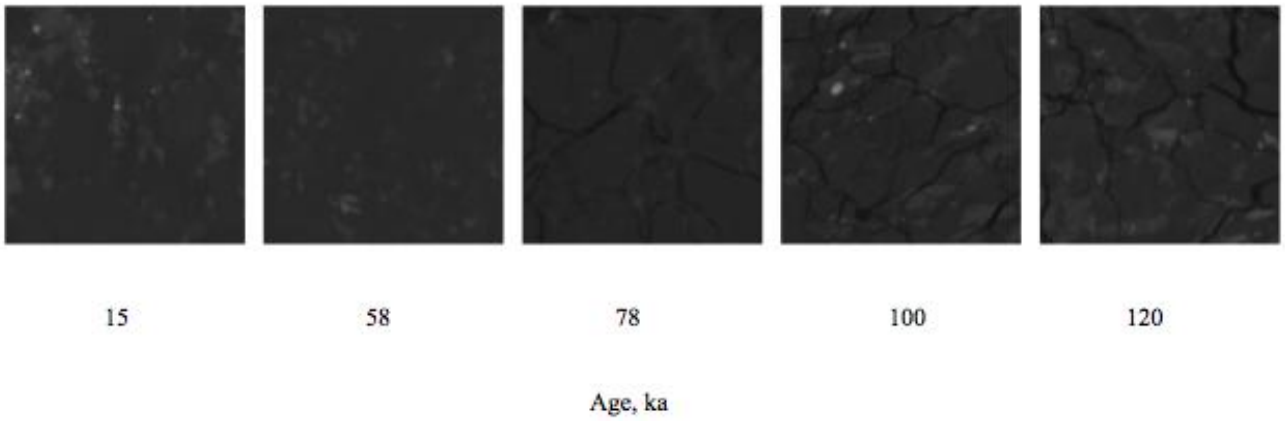

Figure 6. Computed tomography images showing fracture development as a function of rock weathering age.

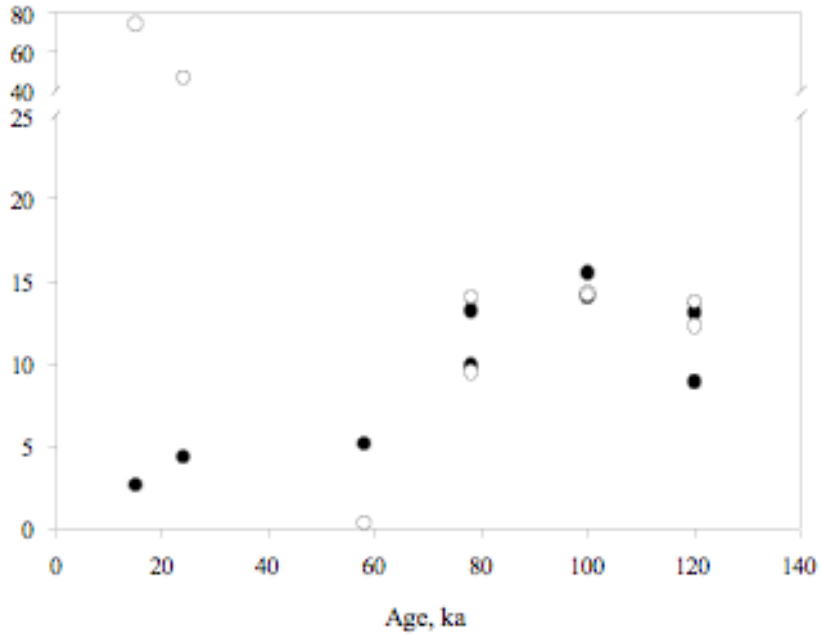

Figure 7. Relationship between age and porosity measured by bulk density (filled circle) and CT-3DMA (empty circle) for rock samples.

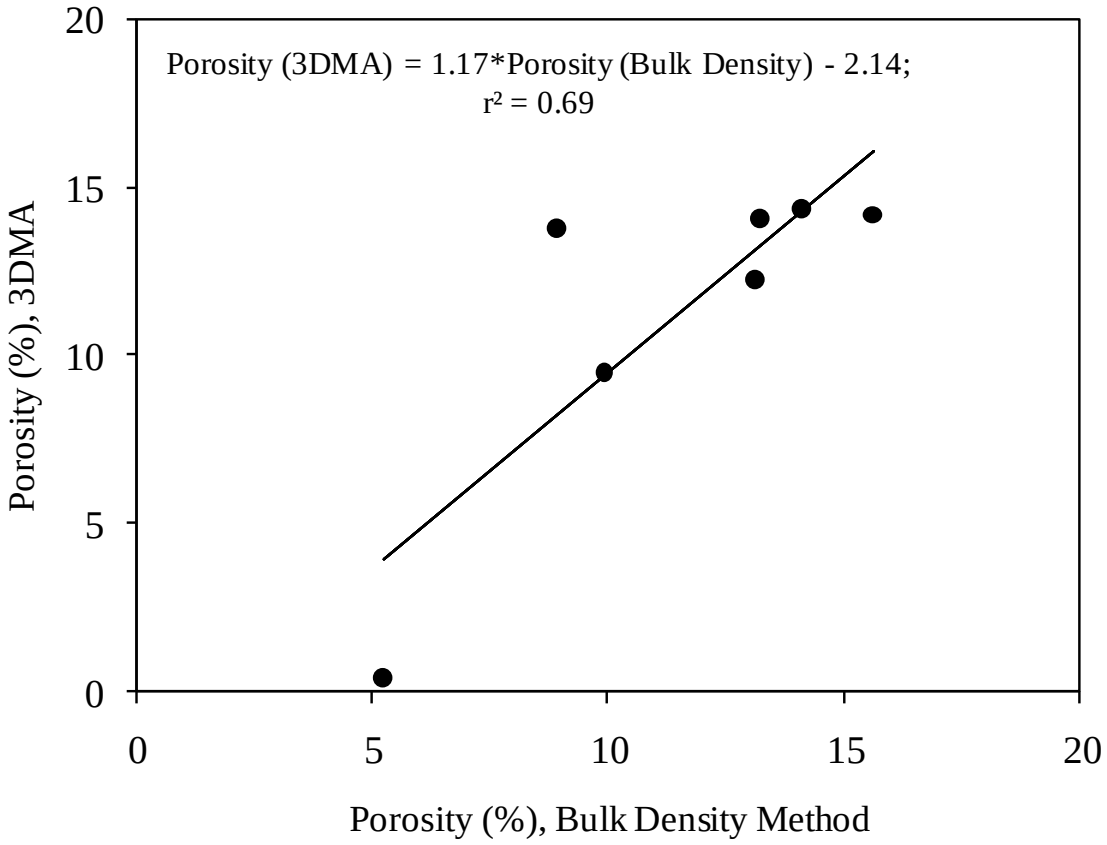

Figure 8. Relationship between porosity measured by the bulk density and CT-3DMA methods.

Pore connectivity is a topological property of the pore space that is crucial for fluid transfer processes. In this analysis, only clast samples from three of the moraines (surface ages 78, 100, and 120 ka) were evaluated because the clasts from the younger moraines (15, 24, and 58 ka) were improperly resolved by the 3DMA procedure. Coordination numbers (CN) were different among the samples and were smaller (<16) for the rock samples. Soil samples had pores with greater CN compared to clasts (Fig. 9). This indicates that the soils have better pore connectivity. Among the four samples shown in Figure 9, the soil sample had 29 clusters and the CN for those clusters ranged from 3 to 35. In contrast, the 78 and 120 ka rock samples had only 12 clusters each, with CN varying between 3 and 16, and the 100 ka rock sample had only 14 clusters with a CN range of 3 to 16. Although CN > 10 does not mean much in terms of pore connectivity as pore size or channel length approach the voxel resolution (Lindquist et al., 2000), the lower CNs for rock samples as compared to soils is an indication of underdeveloped pore networks.

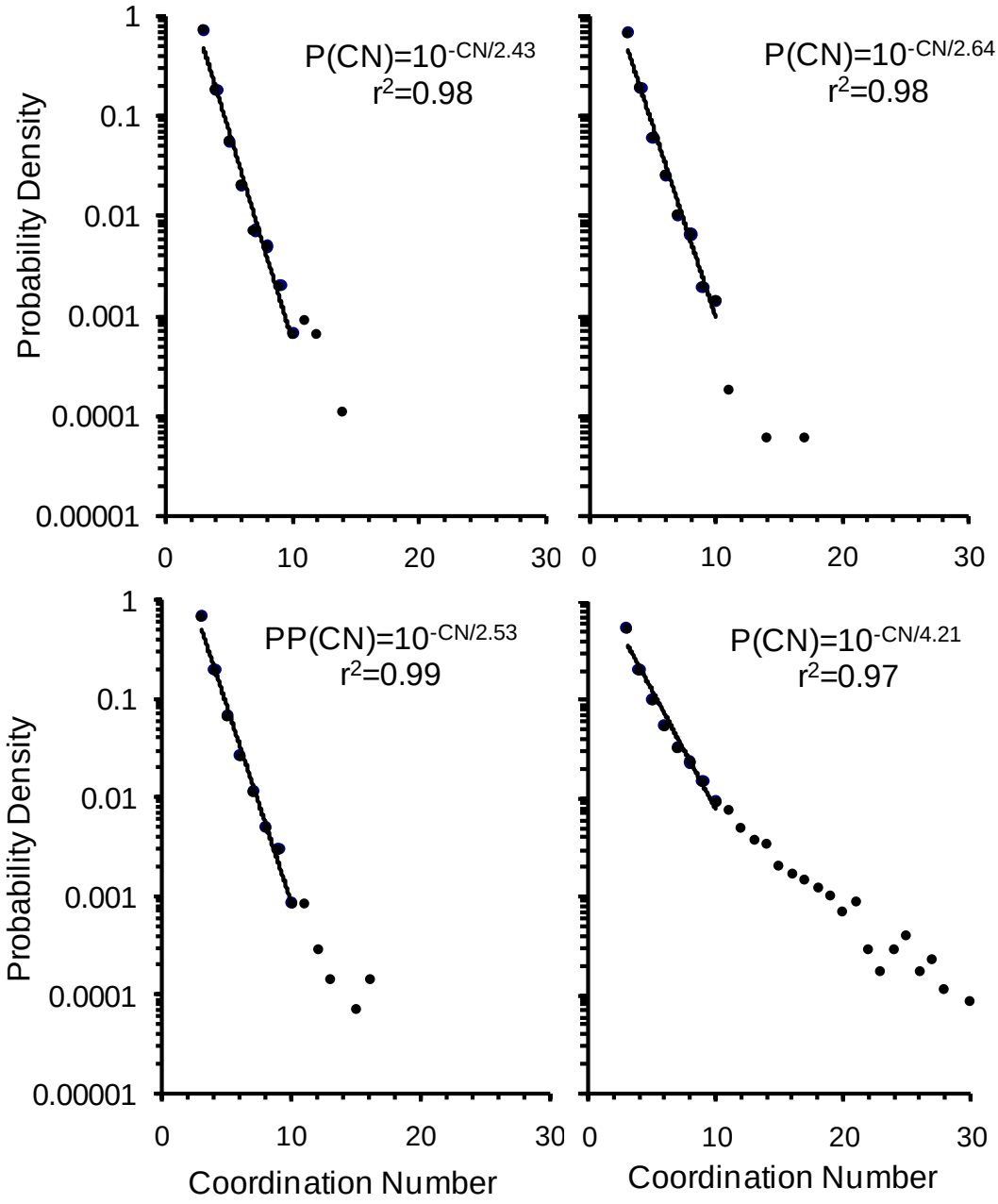

Figure 9. Probability density distributions versus coordination numbers for 78-, 100-, and 120-ka age rock and 100-ka soil samples. The value in the equation is the characteristic coordination number constant (Co).

The probability density for low CN pores varied among samples. However, CN values 1 and 2 were excluded as there are no CN-1 pores and a pore with CN-2 is a part of a pore channel. Pores with CN >10 occur where pore size of the channel length approaches the voxel resolution (Lindquist et al., 2000). Compared to soil samples, weathered clasts had fewer pores, they were less connected, and the probability densities were lower for larger CN pores. Coordination numbers between 3 and 10 were selected for the development of exponential relationships

[$P(CN) \sim 10^{-CN/Co}$; Fig. 9] which results in a characteristic coordination number (Co) for each sample. This range consistently results in an exponential distribution (Lindquist et al., 2000; Udawatta et al., 2008). The relationship between probability and CN was significant and coefficients of determinations were > 97%. As samples develop more connected pores, the Co increased. The average Co for clasts from moraines with surface ages of 78, 100, and 120 ka were 2.49, 2.52, and 2.68, respectively. Differences between clasts by moraine surface ages were not significant at $\alpha = 0.0001$. The average Co for the soil samples was 4.31, which is significantly different from the Co values for the clasts (2.53).

Pore path lengths were similar among the clast samples from the 78, 100 and 120 ka moraines, with longest path lengths ranging from 5.68 to 6.33 mm (Fig. 10). The longest path length in the soil material was 8.82 mm.

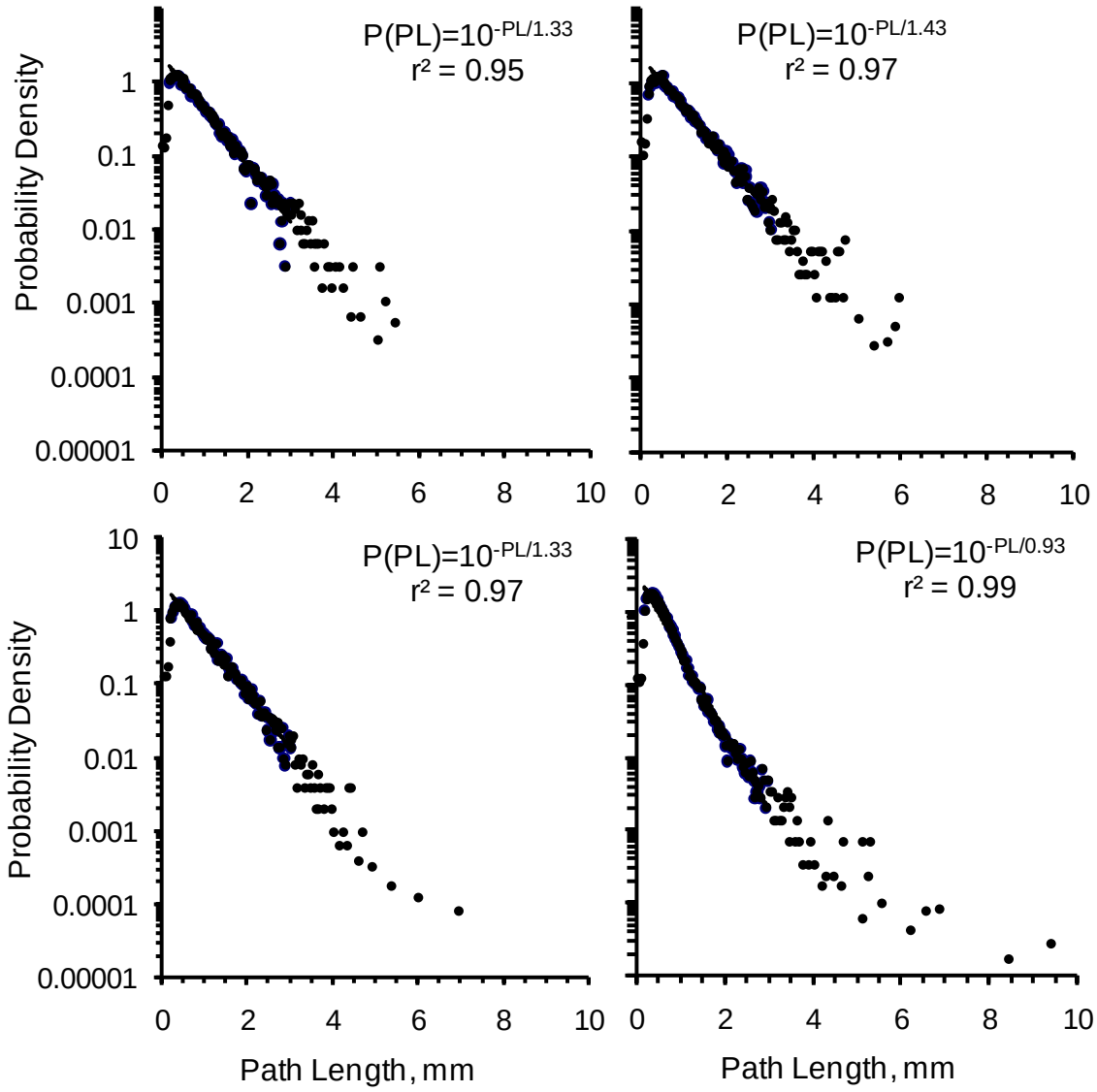

Figure 10. Probability density distributions versus path lengths for 78-, 100-, and 120-ka age rock and 100-ka soil samples.

Pore volume and probability distributions were evaluated to examine effects of weathering on these two parameters among treatments (Fig. 11). Replications of clasts sampled from the same moraine showed almost identical distributions of pore volumes with associated probabilities, except for the two clasts from the 78 ka moraine. The mean pore volume of all six clast samples was 0.069 mm^3 and for the two soil samples was 0.061 mm^3.

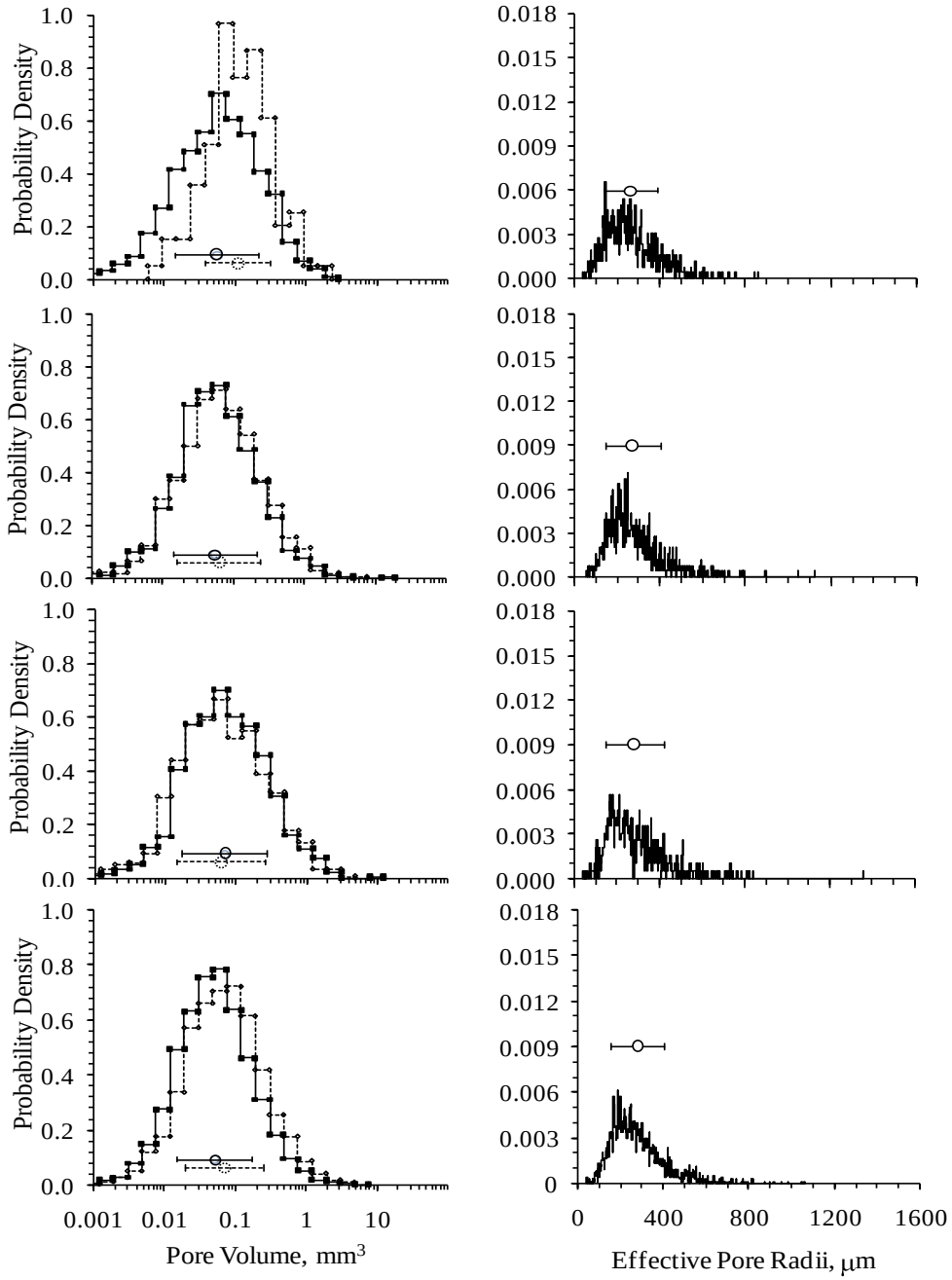

Figure 11. Probability density distributions versus pore volumes for two replications within a treatment (left) and effective pore radii for the selected replicate within a treatment (right) for 78-, 100-, and 120-ka age rock and two soil samples. Horizontal lines indicate the 95% confidence interval and the circle indicates the mean for the replicate.

Effective pore radii were estimated from the erosion procedure acting on thin sections as described by Lindquist et al. (2000) and not from the mean pore volumes. Pore radius is a main factor affecting hydraulic conductivity (Rezanezhad et al., 2009). There were no significant differences in mean pore radii with moraine surface age. Mean pore radii were 290, 267, and 280 μm for clasts from the 78, 100, and 120 ka moraines. The mean pore radii were 270 μm for clasts and 264 μm for soil.

Despite varying path lengths and highly connected pore networks, fluid flow and gas diffusion over longer distances may be impacted by path tortuosity. Figure 12 shows individual pore tortuosity, cumulative tortuosity, and the average values for clasts from the 78 ka, 100 ka, and 120 ka moraines, and the soil from the 100 ka moraine. The mean tortuosity for rock samples had a tight range from 1.34 to 1.36, and the mean soil tortuosity was 1.30. There was no significant difference in tortuosity with duration of clast weathering; however, there were differences between clasts and soil.

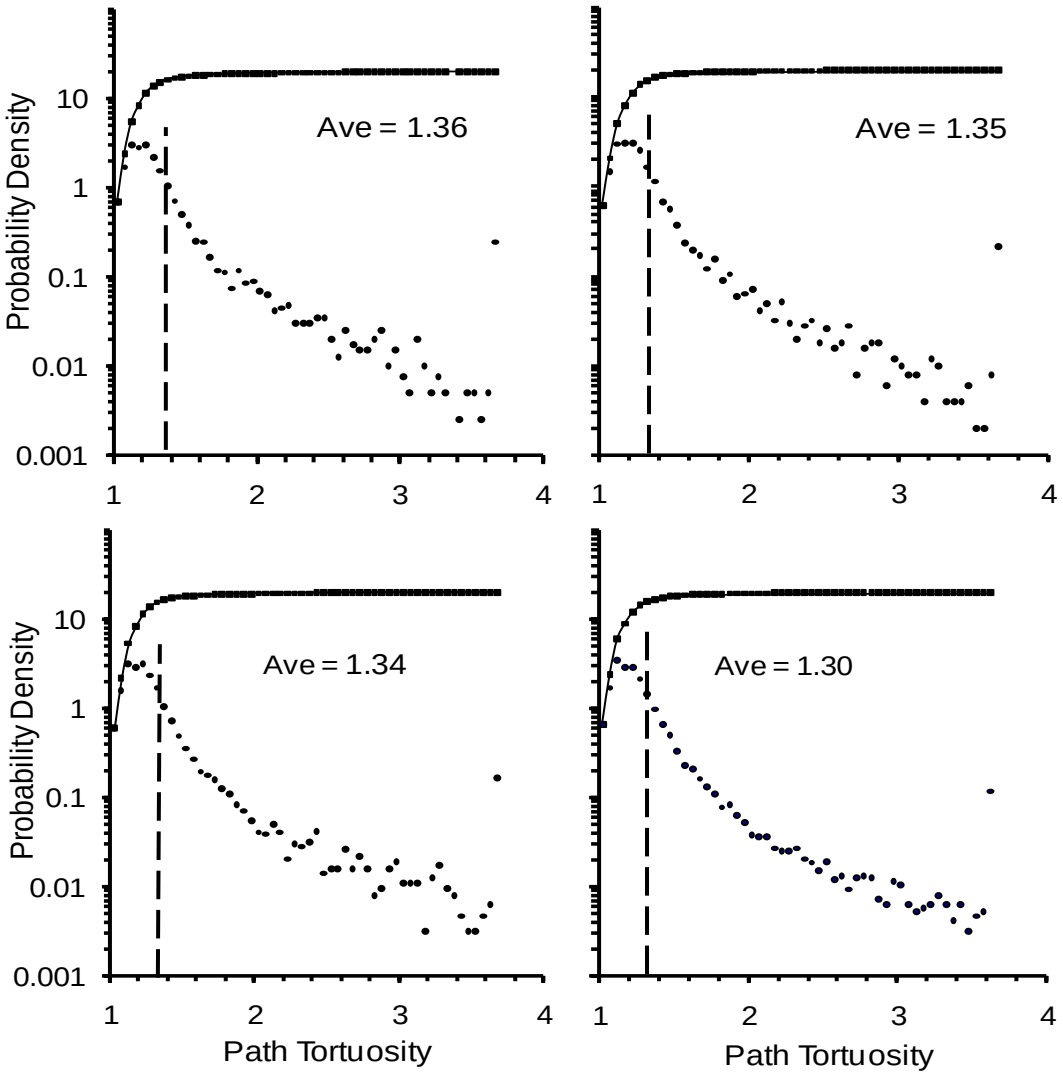

Figure 12. Probability density distributions (solid points) versus path tortuosity and cumulative probability density (solid line) versus path tortuosity for 78-, 100-, and 120-ka age rock and soil samples. Vertical lines indicate the average path tortuosity.

Discussion

Our observations of porosity formation in granitic clasts are consistent with the popular explanation, that the process is driven by expansion of biotite grains. According to this interpretation, oxidation of Fe^{2+} and loss of interlayer K^{+} expands the phyllosilicate structure, opening cleavage planes. Stress induced by the volumetric expansion of biotite shatters the rock, causing inter- and intra-mineral fractures through feldspar and quartz grains (Wahrhaftig, 1965; Isherwood and Street, 1976; Taboada and García, 1999). Over time, micro-cracks expand, propagating through the clasts. Pores become larger, more closely spaced, more interconnected, and have longer less tortuous path lengths as clasts break down to grus. In arid to semi-arid climates, such as the Bishop Creek moraines, grussification of clasts is dominantly a physical process, preceded by only minor chemical weathering (Marchand, 1974). In wetter climates, chemical weathering is more intense and occurs more rapidly, altering primary minerals, forming secondary minerals, and developing greater porosity (Stolt et al., 1991; Vepraskas et al., 1991; Hubbert et al., 2001).

Granitic clasts from older moraines, with increased porosity and better connectivity of pores have the potential for greater water-holding capacity and ease of root and mycorrhizal penetration. The accumulation of illuvial clay films on microfracture walls indicates that water movement has occurred within the clasts. In the Bishop Creek Moraines, we expect that the fine-earth fraction still dominates the ecological functions of the soil, but clasts from the older moraines (e.g., Ta2 and Ta1) have significant porosity that add water-holding capacity and rooting area to the regolith. The contributions of clasts to the soil are likely small at first and increase in time. The transition process and the rate at which it occurs are controlled by the mineralogy of the rock and the active weathering processes determined by environmental factors.

We determined that 10-cm-diameter clasts were fully altered to saprock status after weathering for 81 ka. These clasts held plant-available water and hosted mycorrhizal fungal hyphae; i.e., they were functioning as part of the ecosystem substrate. We use this observation to estimate the rate of ecosystem-functional soil production from granitic bedrock. Since the weathering front moves inward from all sides of the clasts, the weathering thickness is best approximated as the radius. If we assume the clasts to be spherical, this corresponds to a radius of 5 cm. In other words, in 81 ka a rock thickness of 5 cm has been transformed to ecosystem substrate (Rossi and Graham, 2010). This is equivalent to 0.6 mm ka^{-1} of weathering front movement. In contrast, saprolite production from granodiorite in southeastern Australia ranged from 4 to 46 mm ka^{-1}, depending on landscape position (Dosseto et al., 2008). Higher weathering rates in southeastern Australia may be expected due to a higher mean annual precipitation (910 mm yr^{-1}) than in the eastern Sierra Nevada (200 mm yr^{-1}).

We can apply the rates from clast weathering to bedrock weathering, but weathering fronts in granitic bedrock are generally not smooth planar features immediately below the soil. Instead, they typically occupy a wide zone defined by the depth to which meteoric waters penetrate; i.e., the vadose zone. Within this zone, weathering proceeds from the joint fractures into the rock matrix bounded by the joints (Fig. 13) (Frazier and Graham, 2000), so that the entire volume of bedrock within the vadose zone is attacked by weathering, not just at the soil-rock interface. This pattern in which bedrock blocks are weathered from all sides by water percolating through joint fractures is similar to the manner in which clasts are weathered in a moraine.

The vadose zone in residual profiles of granitic rock in the southern Sierra Nevada and the Peninsular Ranges in California is at least 4-m deep (Arkley, 1981; Sternberg et al., 1996; Hubbert et al., 2001) and may be over 8-m deep, judging from root distributions (Hellmers et al., 1955). Joint spacings in granitic bedrock in southern and central California are often on the order of 50 cm (Wahrhaftig, 1965; Sternberg et al., 1996; Witty et al., 2003). Based on the granitic clast weathering rates calculated above (0.6 mm ka^{-1}), hard granitic bedrock with joints spaced 50 cm apart could be weathered to saprock in about 400 ka. The rate of saprock production would be 0.01 mm yr^{-1} if the rock weathering zone was four meters thick, or would be 0.02 mm yr^{-1} if it was eight meters thick. The rate would also be higher where joint spacings are closer; for example, if joints were spaced 25 cm apart and the bedrock weathering zone was 8 m thick, the rate of saprock production would be 0.04 mm yr^{-1}. These rates (0.01 – 0.04 mm yr^{-1}) that take into account simultaneous weathering throughout the vadose zone are similar to the southeastern Australia saprolite production rates (0.004 – 0.046 mm yr^{-1}) calculated by Dosseto et al. (2008). A more accurate comparison of rates would require the use of comparable sampling methods that take into account jointing and other rock morphological features.

This research measured the rate and characteristics of porosity production caused by weathering of granitic rock. From our results, we interpreted the relationships among the different size pores, water movement, weathering mechanisms, and biological habitation. We were somewhat surprised at the minimal evidence of chemical weathering exhibited by mineral grains, even in the most disaggregated rocks from the oldest moraines. Future work should examine porosity formation during clast weathering in moraines of a more humid climate. We would expect more feldspar and mica alteration to clay minerals in those clasts, resulting in finer and more abundant pores.

References

Anand, R.R., and M. Pain. 2002. Regolith geology of the Yilgarn Craton, Western Australia: Implications for exploration. *Australian Journal of Earth Science.* 49:3-162.

Arkley, R.J. 1981. Soil moisture use by mixed conifer forest in a summer dry climate. *Soil Science Society of America Journal.* 45:423-427.

Bullock, P., N. Fedoroff, A. Jongerius, G. Stoops, and T. Tursina. 1985. *Handbook for Soil Thin Section Description.* Waine Research Publications, Wolverhampton, UK.

Dosseto, A., S.P. Turner, and J. Chappell. 2008. The evolution of weathering profiles through time: New insights from uranium-series isotopes. *Earth and Planetary Science Letters*. 274:359-371

Frazier, C.S., and R.C. Graham. 2000. Pedogenic transformation of fractured granitic bedrock, southern California. *Soil Science Society of America Journal.* 64:2057-2069.

Hellmers, H., J.S. Horton, G. Juhren, and J. O'Keefe. 1955. Root systems of some chaparral plants in southern California. *Ecology*. 36:667-678.

Hubbert, K.R., J.L. Beyers, and R.C. Graham. 2001. Roles of weathered bedrock and soil in seasonal water relations of *Pinus jeffreyi* and *Arctostaphylos patula*. *Canadian Journal of Forest Research.* 31:1947-1957.

Isherwood, D. and A. Street. 1976. Biotite-induced grussification of the Boulder Creek Granodiorite, Boulder County, Colorado. *Geological Society of America Bulletin.* 87:366-370.

Lindquist, W.B. 1999. *3DMA General Users Manual.* SUNY-Stony Brook technical report SUNYSB-AMS-99-20. Stony Brook, N.Y.

Lindquist, W.B., and A.B. Venkatarangan. 1999. Investigating 3D geometry of porous media from high resolution images. *Physics and Chemistry of the Earth (A).* 25: 593-599.

Lindquist, W.B., A.B. Venkatarangan, J.H. Dunsmuir, and T.F. Wong. 2000. Pore and throat size distributions measured from synchrotron X-ray tomographic images of Fontainebleau sandstones. *Journal of Geophysical Research.* 105B: 21509-21528.

Lindquist, W.B., S.M. Lee, W. Oh, A.B. Venkatarangan, H. Shin, and M. Prodanovic. 2005. *3DMA-Rock A Software Package for Automated Analysis of Rock Pore Structure in 3-D Computed Microtomography Images.* [Online]. Available at http://www.ams.sunysb.edu/~lindquis/3dma/3dma_rock/3dma_rock.html (verified Nov. 2009). Department of Applied Mathematics and Statistics, SUNY at Stony Brook, Stony Brook, N.Y.

Marchand, D.E. 1974. *Chemical Weathering, Soil Development, and Geochemical Fractionation in a Part of the White Mountains, Mono and Inyo Counties, California.* USGS, Washington, DC.

Phillips, F.M., M. Zreda, M.A. Plummer, D. Elmore, and D.H. Clark. 2009. Glacial geology and chronology of Bishop Creek and vicinity, eastern Sierra Nevada, California. *Geological Society of America Bulletin*. 121:1013-1033.

Rezanezhad, F., W.L. Quinton, J.S. Price, D. Elrick, T.R. Elliot, and R.J. Heck. 2009. Examining the effects of pore size distribution and shape on flow through unsaturated peat using 3-D computed tomography. *Hydrology and Earth System Sciences*. 13: 1993-2002.

Rossi, A.M., and R.C. Graham. 2010. Weathering and porosity formation in sub-soil granitic clasts, Bishop Creek Moraines, California. *Soil Science Society of America Journal.* 74:172-185.

SAS Institute. 1999. *SAS user's guide. Statistics.* SAS Inst., Cary, NC.

Sternberg, P.D., M.A. Anderson, R. C. Graham, J.L. Beyers, and K.R. Tice. 1996. Root distribution and seasonal water status in weathered granitic bedrock under chaparral. *Geoderma.* 72:89-98.

Stolt, M.H., J.C. Baker, and T.W. Simpson. 1991. Micromorphology of the soil-saprolite transition zone in Hapludults of Virginia. *Soil Science Society of America Journal.* 55:1067-1075.

Taboada, T. and C. García. 1999. Pseudomorphic transformation of plagioclases during the weathering of granitic rocks in Galicia (NW Spain). *Catena.* 35:291-302.

Udawatta, R.P., C.J. Gantzer, S.H. Anderson, H.E. Garrett. 2008. Agroforestry and grass buffer effects on high resolution X-ray CT-measured pore characteristics. *Soil Science Society of America Journal.* 72: 295-304.

Vepraskas, M.J., A.G. Jongmans, M.T. Hoover, and J. Bouma. 1991. Hydraulic conductivity of saprolite as determined by channels and porous groundmass. *Soil Science Society of America Journal.* 55:932-938.

Wahrhaftig, C. 1965. Stepped topography of the southern Sierra Nevada, California. *Geological Society of America Bulletin*. 76:1165-1190.

Witty, J.H., R.C. Graham, K.R. Hubbert, J.A. Doolittle, and J.A. Wald. 2003. Contributions of water supply from the weathered bedrock zone to forest soil quality. *Geoderma.* 114:389-400.

This research was funded by the Kearney Foundation of Soil Science: Understanding and Managing Soil-Ecosystem Functions Across Spatial and Temporal Scales, 2006-2011 Mission (http://kearney.ucdavis.edu). The Kearney Foundation is an endowed research program created to encourage and support research in the fields of soil, plant nutrition, and water science within the Division of Agriculture and Natural Resources of the University of California.